Lasers in Manufacturing Conference 2015

3D weld seam characterization based on optical coherence tomography for laser-based thermal joining of thermoplastics to metals

Robert Schmitt[a,b], Guilherme Mallmann[a] , Philippe Ackermann[a,]*, Jean Pierre Bergmann[c], Martin Stambke[c], Klaus Schricker[c]

[a] *Fraunhofer Institute for Production Technology IPT, Steinbachstraße 17, Aachen, Germany*
[b] *Laboratory for Machine Tools and Production Engineering WZL, RWTH Aachen University, Steinbachstr. 53, Aachen, Germany*
[c] *Technische Universität Ilmenau, Department of Production Technology, Gustav-Kirchhoff-Platz 2, Ilmenau, Germany*

Abstract

Laser-based thermal joining of metals to plastics shows a great potential for functional constructions especially in terms of light weight design. Thereby, the process strategy and time-temperature regime affects the resulting joint zone; hence process monitoring is a central issue. State of the art monitoring and quality assurance systems for this technology are limited as no direct information about the joining zone itself is given. Within this paper, a new method for the quality assurance in metal-plastic hybrids is presented using optical coherence tomography (OCT). This approach enables the measurement of the joint geometry as well as bubbles, imperfections and the wetted bonding area.

Keywords: optical coherence tomography, metal-plastic joining, laser-based thermal joining, process monitoring and control

1. Introduction and State of the Art

Lightweight design gains importance in automotive industry and aviation industry as well as in mechanical engineering generally. The main motivations are legal requirements, environmental aspects and a reduced mass of moving parts, e. g. in machine-tools. One approach in engineering constructions for achieving these

* Corresponding author. Tel.: +49-241-8904-540; fax: +49-241-8904-6540.
E-mail address: philippe.ackermann@ipt.fraunhofer.de.

purposes is the use of multi-material design for a reduction of mass by increasing the functional density, fatigue behavior, stiffness or loading capacity. The use of the right material at the right place enables the realization of this approach. Thereby, a great potential is shown by the use of metal-thermoplastic hybrid joints. On the one hand, thermoplastics show advantages concerning freedom of design and a high rigidity by using fiber-reinforced plastics. On the other hand, metals are used in structural parts and are advantageous regarding ductility. However, multi-material design shows demanding requirements on joining technology as key enabler for the application of metal-thermoplastic joints. In joining technologies, the use of an additional material, connecting elements or direct joining is possible. Additional materials, e. g. adhesives, show disadvantages concerning aging and hardening time. Connecting elements, e. g. rivets or screws are causing local stress concentrations and notching effects. Direct joining avoids these disadvantages and enables an areal bonding between metal and thermoplastic as well as a high joint strength. Direct joining is a thermal process which requires a sufficient energy input for melting the thermoplastic at the boundary layer between metal and plastic by heat transmission. Afterwards, the molten polymer penetrates the surface structures and wets the metal. A permanent joint is formed after solidification.

The energy input can be performed by any energy source, e. g. a conductor (Sickert et al. 2012), an inductor (Roesner et al. 2011), ultrasonic (Balle et al. 2012) or laser radiation (Katayama et al. 2012). The laser process shows advantages over competitive processes by a locally limited energy input and a geometrically independent joining zone. The process can be carried out as heat conduction or transmission joining (Katayama et al. 2012), depending on arrangement of joining partners. Thus, the process arrangement leads to a typical time-temperature profile of the laser process which influences the resulting joint and its behavior (Schricker et al. 2015). A sufficiently long period of time within the working-temperature range is necessary to achieve a complete wetting of the metal surface and to avoid interruptions within the joining zone. On the other hand, a long duration of high temperatures can cause degradation of the polymer (Katayama et al. 2012). Thereby, decomposition products from the plastic material and/or the evaporation of dissolved water can lead to bubble formation within the joining zone and a decrease of joint strength.

Key criteria for process quality management do not exist yet, neither a specific quality assurance process. Those factors could improve product quality and process security by recording the above mentioned points or other characteristic parameters. Current monitoring systems for this purpose are based on the detection of the electromagnetic radiation emitted from the joint area (thermal imaging cameras or IR-pyrometers), position and displacement sensors, force measurements sensors and finally destructive methods (Haberstroh et al. 2014, Kah et al. 2013). These systems do not deliver direct information about the joint geometry or the appearance of bubbles during the process.

In order to solve these issues, an optical measurement system based on optical coherence tomography (OCT) is presented. OCT, originally introduced and used for the contactless depth-resolved imaging of biological tissues (Huang et al. 1991), is used more and more outside biological applications. The advantage of a contact-free, non-invasive and non-destructive evaluation of materials via 1D up to 3D-image data is used in a growing number of applications. The potential of this system has been recognized already within the early years after it has been invented (Swanson et al. 1996). An overview on OCT applications outside biomedicine was published by Stifter et al. 2007. Recent examples for non-destructive testing and evaluation (NDTE) were shown for weld seam characterization in the process of laser transmission welding of polymers (Schmitt et al. 2014). Thereby, the created data include e. g. the thickness of layers as well as the size and distribution of pores, fibers or cells. By using image processing tools, it is possible to automatically analyze

sample features. Qualitative information is obtained through the visual inspection of the acquired images. Features like surfaces or impurities can easily be detected and give rapid indications on the condition of the sample. Nowadays, several companies and research centers are offering commercially available OCT systems or prototypes for applications outside the medical sector and the common optics laboratory. In the field of NDTE, the development of commercially available OCT systems is customized towards the investigation of one particular kind of sample. So far, adequate parameters for any kind of process-related adaptation have not yet been identified (Haberstroh et al. 2014). The features of the previously mentioned OCT technology provide a new tool for both quantitative and qualitative information of workpiece and process in metal-plastic hybrid thermal joining processes as well as in applications involving semi-transparent materials.

2. Theoretical principles of the spectral domain-optical coherence tomography (SD-OCT)

SD-OCT is based on low-coherence interferometry where the depth information is obtained by analyzing the spectrum of an acquired interferogram. The output from a broad-bandwidth light source is split into two beams. One beam is aimed towards the sample and is reflected back or backscattered from internal structures at different depths. The second beam is reflected from a reference mirror with fixed position. Both beams are further recombined and interfere with each other. The generated interference is finally acquired by a spectrometer. The Fourier transformation of the acquired spectrum provides a backreflexion profile as a function of depth. Depth information is obtained by the different interference profiles from different pathlengths in both arms. Larger differences in the optical pathlength between the sample and the reference arm result in higher frequency interference signals. At the spectrometer´s line scan detector, the different wavenumbers result from the combined signal of both arms (Brezinski 2006, Drexler et al. 2008). Figure 1 depicts a standard SD-OCT setup.

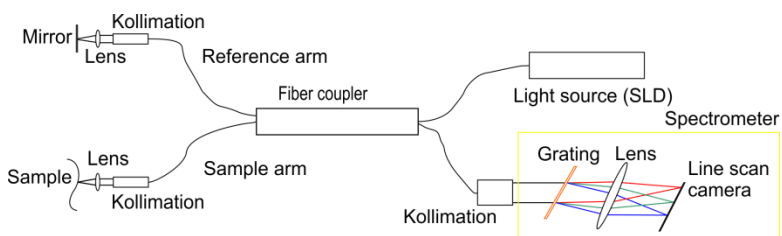

Fig. 1. Schematic representation of a SD-OCT setup

Spectrum analysis is performed via the means of a spectrometer. The light is separated into the spectral components by a diffraction grating and afterwards, the spectrum is imaged on a line scan detector. The maximum measurement depth of the OCT system depends on the highest spatial frequency that can be measured by the spectrometer (Hagen-Eggert et al. 2012).

The total interference signal *I(k)* is given by the spectral intensity distribution of the light source (*G(k)*) times the square of the sum of the two back reflected signals. a_R being the reflection coefficient of the reference arm and *a(z)* the backscattering coefficient of the object (with regard to the offset z_0 between reference plane and object surface), where k is the optical wavenumber (Brezinski 2006).

$$I(k) = G(k)\left|a_R \exp(i2kr) + \int_{z_0}^{\infty} a(z)\exp\{i2kn(z)(r+z)dz\}\right| \quad (1)$$

Where n is the refractive index, *2r* is the path length in the reference arm, *2(r+z)* is the path length in the object arm and *2z* the difference in path length between both arms. By finding the maximum amplitude of the spectrum using Fourier transformation, the absolute optical path difference can be detected. The maximum measuring depth (Z_{max}) is described by (Tommlings et al. 2005).

$$Z_{\max} = \left(\lambda_0^2 / 4n\Delta\lambda\right)N \tag{2}$$

Where λ_0 is the central wavelength, $\Delta\lambda$ is the bandwidth, n is the samples refractive index and N is the number of detector units covered by the light source spectrum. The axial resolution of a FD-OCT is described by (Tommlings et al. 2005).

$$AR_{FD-OCT} = l_c / 2 \approx 0.44\,\lambda_0^2 / \Delta\lambda \tag{3}$$

For single distance measurements (a single back reflection), the axial resolution can be increased to a sub-micrometric resolution by the usage of signal processing techniques, e. g. gauss fit. Within SD-OCT, superluminescent diodes are used as low coherent light sources. These light sources are available with central wavelengths from 650 nm to 2100 nm, different output power levels and spectral bandwidths. This enables a high flexibility of the system design regarding optimization for the application. OCT images can be either obtained as a single depth measurement (called A-Scan), as slice images (called B-Scan, where a sequence of A-Scans from different vertical or horizontal positions is added up) or as volumetric images (called C-Scan, where a sequence of B-Scans from different positions is added up).

3. Objective

In this paper, OCT is used for the analysis of laser manufactured metal-plastic hybrid joints. This method will be used to characterize the joint geometry as well as the quality of the joint, thus delivering quantitative values of the joint geometry for the selected parameters. Bubble formation (A), an interrupted joining zone (B) and melt ejection (C) at the edge of the lap joint were considered as determining factors (see Fig. 2). Bubbles and their influence were discussed previously. An interruption within the joining zone is an area without wetting between plastic and metal and a potential flaw. Using this method, even the size of spot joints can be determined. As a last parameter, the melt ejection was chosen as possible factor for non-destructive quality tests which can be examined for plastics with low transparency.

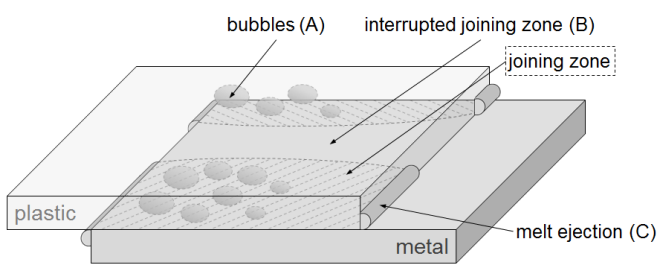

Fig. 2 Schematic view of the joint with bubbles (A), an interrupted joining zone (B) and melt ejection (C)

Based on these three parameters, the usability of OCT for non-destructive testing of metal-plastic hybrid joints will be demonstrated using different thermoplastic materials and process parameters. Subsequently, a solution concept for online process monitoring based on OCT and integrated within the laser-based joining process will be presented.

4. Experimental Setup

4.1. Laser-based thermal joining

The experimental investigations for laser-based joining were carried out as heat conduction process on a fiber-coupled diode laser (Laserline LDM 3000, λ = 980 nm) with top heat intensity distribution. A schematic view of the overlap joint is shown in Fig. 3a. As joining parameters, a constant beam power of 1 kW (dwell time at process start: 8 s) and a focal diameter of 6 mm were used. The joining pressure was constant at 0.5 $N \cdot mm^{-2}$. The laser was active for 80 mm because of heat accumulation at seam start and end. The joining speed was varied in an interval from 2 up to 4 $mm \cdot s^{-1}$ in order to adjust a varying bubble size and distribution within the joint zone. As materials, an aluminum alloy EN AW 6082 (according to DIN EN 573-3, dimensions: 75 x 100 x 1.5 mm^3) was used as metal joining partner as well as semi-crystalline Polyamide 6.6 (Nylon 6.6, PA 6.6) and amorphous Polycarbonate (PC) as thermoplastic joining partners (dimensions: 75 x 100 x 2 mm^3). Before the process, the metal surface was prepared by a laser ablation process to create line-shaped structures in joining direction (structure density: 28 $lines \cdot mm^{-1}$, depth: 30 µm, width 25 µm by Rofin PowerLine F20). For generating an interrupted joining zone as emulated defect, the laser process (joining speed: 2 $mm \cdot s^{-1}$, PA 6.6) was paused between 50 mm and 70 mm to decrease heat input and cause imperfections in the wetting behavior. This setup allows the adjustment of bubble distribution and melt ejection depending on varied joining speeds as well as the examination of an interrupted joint zone.

4.2. OCT setup and measurement strategy

A standalone OCT system was used as a qualification tool for the characterization and quantification of hybrid joints manufactured by laser-based thermal joining. The measurement system used a superluminescent diode with a central wavelength at 1325 nm and a spectrum bandwidth of 150 nm. A line camera was used to acquire the modulated light spectrum. The axial resolution, refractive index dependent, is below 7.5 µm and the lateral resolution is 15 µm in air. In the experiments, each volume consists of 512 x 512 x 302 pixels, corresponding to a material volume of 5.5 mm x 5.5 mm x 1.497 mm (Length x width x depth). The present OCT images represent backscattered reflections in greyscale from the upper surface of the metal component as well as the lower part from the plastic component, covering an area of 1.497 mm depth and positioned within the interference region. The joint is formed after wetting the metal surface and penetrating the surface structures by molten polymer, thus a reflection is generated and the joint zone can be measured. Bubbles and imperfections also generate reflections and are represented in the tomographical pictures. The volumetric point clouds as well as slices of these volumes were analyzed for the characterization. Comparative measurements by X-ray test (General Electric phoenix nanome|x 180) and microsections were made at the same positions. Fig. 3a shows a schematic view of the hybrid metal-plastic component and the areas where the OCT measurements were performed for detecting the named criterions for bubble formation (A), melt ejection (B) and interrupted joining zone (C). In Fig. 3b, a picture of the joining zone (top view) and the related OCT image (5.5 mm x 5.5 mm) is shown. Fig. 3c displays an OCT slice image from the plastic-metal overlap edge (B). The OCT images are based on 512 slice images, the false-color images are based on the final volumetric point cloud for correlating depth information to a color scale.

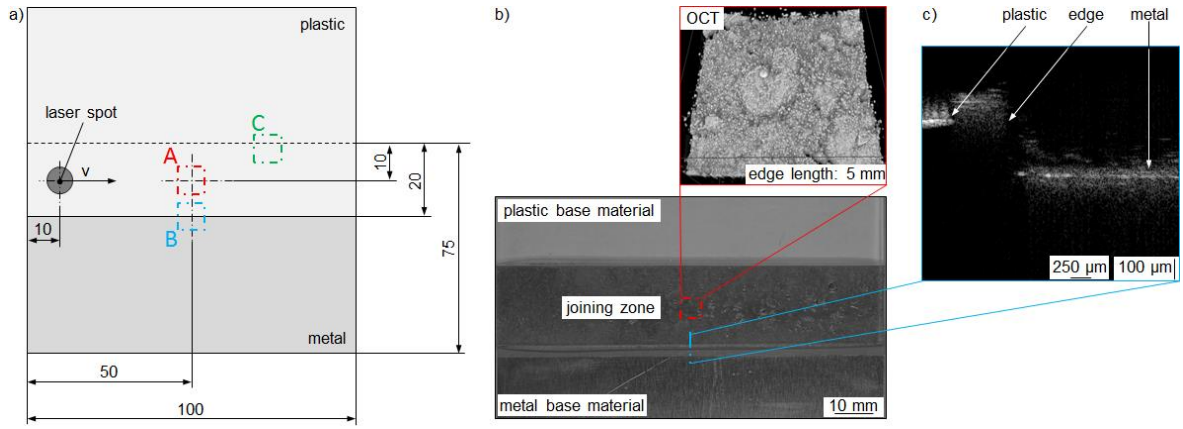

Fig. 3. a) Schematic view of measurement areas for bubbles (A), melt ejection (B) and interrupted joining zone (C); b) example top view of specimen and sampled 3D OCT-image; c) example surface slice

5. Results

5.1. Detection of bubbles within the melting layer

In this step, the joining zone of the aluminum-polycarbonate hybrid is analyzed concerning bubbles. For this consideration, both volumetric and slice measurements are carried out and the distribution of the bubbles can be analyzed via image processing. The measured area (A) according to bubble formation is shown in Fig. 4. For a better presentation, the point cloud data based on OCT images have been shown in 3D imaging for false-color plots. The different bubble sizes and their distribution in depth as well as other structures can be identified clearly according to the joining speed of the laser process. Based on Fig. 4, the size of the bubbles decreases significantly from large, agglomerated bubbles to a fine distribution by increasing the joining speed due to a reduced thermal load of the plastic.

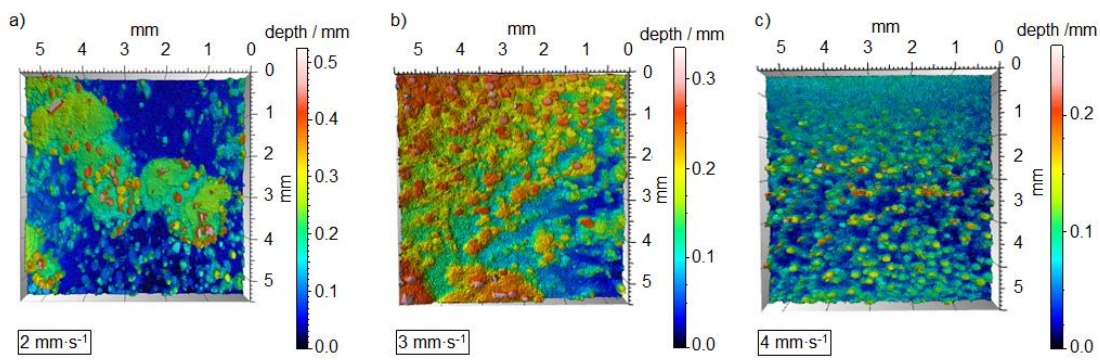

Fig. 4. 3D Overview mapping of the joining zone as false-color plots for comparison of bubble formation between joining speed a) 2 mm·s^{-1}, b) 3 mm·s^{-1} and c) 4 mm·s^{-1} (PC)

The number of bubbles according to z-position (depth) is analyzed via an Abbot-Firestone curve (Fig. 5) based on the generated volumetric point cloud measurements. The thermal distortion of both materials was

compensated during material distribution analysis by a software-based reference layer. The depth histogram in Fig. 5 is used for analyzing the bubble distribution of the analyzed area. The vertical axis shows the depth into the material and the horizontal axis (bottom) shows the percentage of the material distribution for the depth histogram. The Abbott-Firestone curve (depicted red) displays the percentage of contact area or passed material in relation to the passed area from the highest peak on as starting point. The top horizontal axis represents the percentage contact area denoted by the Abbott curve. These figures give a statement about the actual bubble concentration per volume for the analyzed area of 5.5 mm x 5.5 mm x 1.497 mm within the joining zone for the different joining speeds. These tools can be easily used as a tolerance analysis in production for the qualification of thermally joined components. Statements about the number of bubbles are rather difficult to perform, but a general volume consideration of the material and the void material (bubbles) can be performed with the mentioned histogram and the Abbott curve. In further investigations, a threshold could be established by comparison of specimens without bubbles and components within a limited value of bubbles, to reduce the scrap rate in correlation to the laser process.

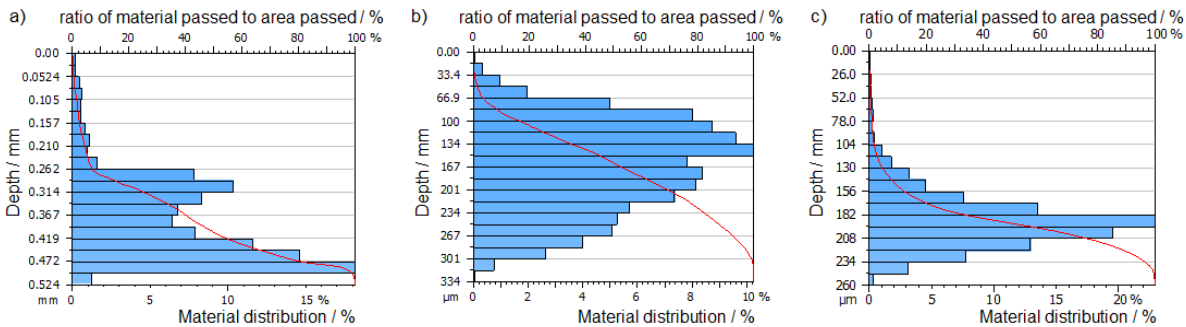

Fig. 5 Depth histogram of material distribution (blue) and Abbott-Firestone curve (red) for a) 2 mm·s^{-1}, b) 3 mm·s^{-1}, c) 4 mm·s^{-1}

Based on these results, a correlation between joining speed and bubble concentration depending on material depth can be assumed (Fig. 5a-c). For a low joining speed (Fig. 5 a), the bubbles are located in a higher region regarding the boundary layer between plastic and metal because of a higher flowability of the thermally influenced plastic. For higher joining speeds (Fig. 5 b, c) the position is decreased by the limited flowability of the plastic. The shift of the peak and distribution from 2 up to 4 mm·s^{-1} must be considered in future investigations for statistically verified statements.

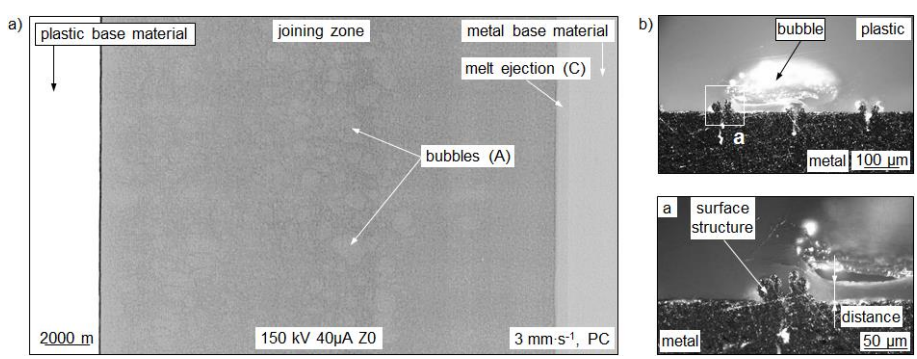

Fig. 6. Comparative measurement by a) X-ray test (PC) and b) microsections at the boundary layer (2 mm·s^{-1}, material PA 6.6)

In comparison to these results, measurements with X-ray test and metallographic investigations on bubbles were made. Fig. 6a shows the bubble distribution over the joining zone for X-ray test, although information in z-direction concerning the position of the bubbles cannot be obtained without using X-ray tomography. The minor contrast between bubbles and surrounding materials is caused by the slight difference in densities. As an example for the bubble position in z-direction, microsections were taken out to evaluate this parameter (see Fig. 6b). Thereby, a thin film of plastic between boundary layer and bubble can be determined, even between completely penetrated surface structures and bubbles. The main reason for this behavior is open and further investigations on the time-depend formation of bubbles are necessary.

5.2. Detection of interrupted joining zone

The analyzed area of the aluminum-polyamide 6.6 hybrid shows the interrupted joining zone between plastic and metal in overlap configuration which was intentionally generated by a temporary interruption of the joining process (see 4.2) to qualify OCT for detecting non-wetted areas at the boundary layer. Fig 7 shows the transition area between joining zone (left) and interrupted joining zone (right). The melt ejection (top left) is attached seamlessly to the joining zone and is located next to plastic base material (top right). Thereby, OCT enables a clear detection of the interrupted zone in the middle of the image due to a small gap between both joining partners. Thereby, the gap was greater or equal than 7.5 µm to be detected via image processing due to the limited resolution of the current experimental setup.

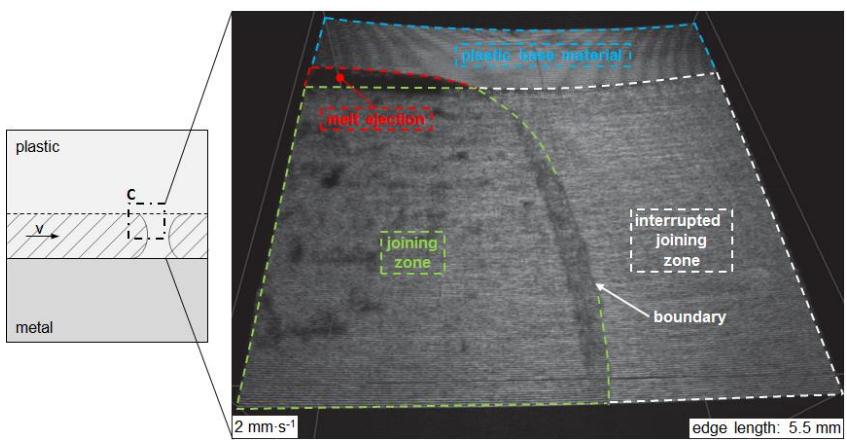

Fig. 7. Interrupted joining zone as an area without wetting between plastic and metal, melt ejection at the joint edge and plastic base material without metal substrate (PA 6.6)

5.3. Detection of melt ejection

The melt ejection at the edge of the metal-polycarbonate hybrid joint is shown in Fig. 8 as 3D view. The plastic material gets molten by the energy input of the laser beam and is partially ejected due to joining pressure. The measurement of this geometrical quantity could be used for visual quality inspection for example. Therefore, this effect occurs for non-reinforced and fiber-reinforced polymers with high fiber-volume content, it could possibly be used as quality criterion for hybrid joints without consideration of material composition. The interruptions in image composition, as seen in Fig. 8, between plastic, ejected

melt and metal surface are caused by shadow effects at the edges. Hence, no light returns to the measurement system.

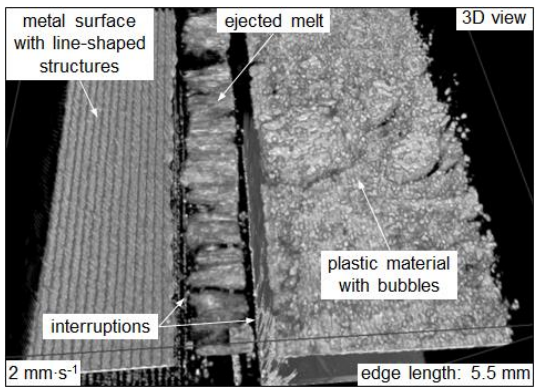

Fig. 8. 3D image of melt ejection between thermoplastic and metal component (PC)

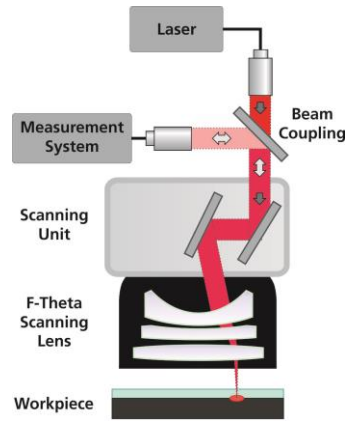

Fig. 9. Example of a control solution concept with laser scanner for transmission welding (schematic view)

5.4. Solution concept for process monitoring

Based on the results in this paper, the realization of a solution concept for process monitoring by the development and integration of a customized OCT systems into the joining process is possible. This allows a tomographical characterization and evaluation of laser-based metal plastic joints. Thereby, the measurement beam and process beam would be coaxially combined (Fig. 9). In case of heat conduction joining the two beams would not be coaxially combined and the measurement system would not be integrated into the existing laser setup. Uncertainties in the process could be avoided by acquiring the tomographic image of the joint in machine coordinates, hence coordinate transformation would be avoided. Prior to any machine integration, the optical characteristics of the scanning system as well as the materials to be joined will have to be characterized. As most laser systems for thermal joining use diode lasers with a wavelength between 808 nm and 980 nm, a measurement system with a central wavelength dependent on the specific used laser wavelength will be preferable for machine integration. This will reduce the overall optical aberrations of the scanning system and optics and simplify the beam coupling. The presented inline measurement device will enable the acquisition of quantitative information from the thermal joining process (geometry, bubbles, imperfections etc.). This will enable new ways for an online control and quality assurance, which are simply not possible with current process monitoring and control technology.

6. Conclusion

The achieved results in this work qualify the OCT technology as a quality assurance tool for metal-thermoplastic joints with the ability to identify and quantify existing bubbles, interruptions and gaps as well as ejected plastic material. Bubbles and their position as well as their distribution within the joining area are clearly detectable at various material depths. An analysis of the bubbles can be performed and has to be correlated to the laser-based process and joint quality in future work. Interruptions within the joining zone can be detected within the minimum resolution of the current experimental setup and allow drawing

conclusions on wetting behavior. The ejection of molten plastic at the joint edge can be measured by the OCT as well and it can serve as a possible quality criterion for hybrid joints. Due to the given technology, the measurement wavelength and the presented solution can be adapted and optimized for different joining applications. There is still a high potential for improvement, e. g. regarding the axial resolution for the bubble detection and also concerning the measurement of plastics containing any kind of glass fiber reinforcements. Finally the integration of the measurement system into the joining process will enable a better understanding of bubble formation and imperfections within the joint. These investigations can support a better modelling of the process and lead to an adaptive and online controlling solution.

Acknowledgements

The authors would like to thank the German Federal Ministry of Education and Research (BMBF) for the support of the project "MANUNET-Weldable" (02PN2011/02PN2012) and the Project Management Agency Karlsruhe (PTKA) as well as the Department of Economy, Employment and Technology (TMWAT) in Thuringia (Germany) and the European Social Fund (ESF) for the support of the project "Thermal Joining of Hybrid Structures" within the research group "Polymer Based Lightweight Composite Materials in Automotive Engineering" (2011FGR0109).

References

Sickert, M.; Haberstroh, E.; 2014. Thermal Direct Joining for Hybrid Plastic Metal Structures. Proceedings of Euro Hybrid Materials and Structures 2014, pp. 42-45.

Roesner, A.; Scheik, S.; Olowinsky, A.; Gillner, A.; Reisgen, U.; Schleser, M.; 2011. Laser Assisted Joining of Plastic Metal Hybrids. Physics Procedia 12, pp. 370-377.

Balle, F.; Eifler, D.; 2012. Monotonic and Cyclic Deformation Behavior of Ultrasonically Welded Hybrid Joints between Light Metals and Carbon Fiber Reinforced Polymers (CFRP). Fatigue Behaviour of Fiber Reinforced Polymers: Experiments and Simulations, DEStech Publications, pp. 111-122.

Katayama, S.; Kawahito, Y.; Mizutani, M.; 2012. Latest progress in performance and understanding of laser welding. Physics Procedia 39, pp. 8-16.

Schricker, K.; Stambke, M.; Bergmann, J. P.; 2015: Adjustment and Impact of the Thermoplastic Microstructure of the Melting Layer in Laser-based Joining of Polymers to Metals. In: Proceedings of Lasers in Manufacturing 2015.

Roesner A., Scheik S., Olowinsky A., Gillner A., Reisgen U., Schleser M., 2011. "Laser assisted joining of plastic metal hybrids", LiM 2011, Physics Procedia 12 [2011] pp. 370-377.

Haberstroh E., Sickert M., 2014, "Thermal direct joining of hybrid plastic metal components", KMUTNB Int. J. Appl. Sci. Technol, Vol.7, No.3, pp. 29-34.

Kah P., Suoranta R., Martikainen J., Magnus C., 2014, "Techniques for joining dissimilar materials: metals and polymers", Rev. Adv. Mater. Sc. 36 (2014) pp. 152-164.

Huang D. et al., 1991, "Optical coherence tomography", Science 254, pp1178–81.

Swanson, E.A., Hee, M.R., Tearney, G.J., Fujimoto, J.G., 1996, "Application of optical coherence tomography in nondestructive evaluation of material microstructure", In Lasers and Electro-Optics, CLEO '96, pp. 326–327.

Stifter, D., 2007, "Beyond Biomedicine: A Review of Alternative Applications And Developments For Optical Coherence Tomography", Applied Physics B 2007, 88, 337–357.

Schmitt R., Mallmann G., Devrient M., Schmidt M., 2014, "3D polymer weld seam characterization based on optical coherence tomography for laser transmission welding applications", 8th International Conference on Photonic Technologies LANE 2014.

Brezinski M., 2006, " Optical coherence tomography, "Principles and Applications"", Elsevier, ISBN 978-0121335700, pp. 130-134.

Drexler W., Fujimoto J.G., 2008, "Optical Coherence Tomography: Technology and Applications", Springer-Verlag Berlin Heidelberg.

Hagen-Eggert M., Koch P., Hüttmann G., 2012, "Analysis of the signal fall-off in spectral domain optical coherence tomography systems", Optical Coherence Tomography and Coherence Domain Optical Methods in Biomedicine XVI, Proc. of SPIE Vol. 8213, 82131K-1.

Tomlings P. and Wang, R., 2005 "Theory, developments and applications of optical coherence tomography", Applied Physics, no. 38, pp. 2519-2535.